Thermal Atomization of Platinum Nanoparticles into Single Atoms: An Effective Strategy for Engineering High-Performance Nanozymes

Yuanjun Chen,[‡] Peixia Wang,[‡] Haigang Hao,[‡] Juanji Hong,[‡] Haijing Li, Shufang Ji, Ang Li, Rui Gao, Juncai Dong, Xiaodong Han, Minmin Liang,* Dingsheng Wang,* and Yadong Li

ACCESS | 📊 Metrics & More | 📖 Article Recommendations | 🆂🅸 Supporting Information

ABSTRACT: Although great progress has been made in artificial enzyme engineering, their catalytic performance is far from satisfactory as alternatives of natural enzymes. Here, we report a novel and efficient strategy to access high-performance nanozymes via direct atomization of platinum nanoparticles (Pt NPs) into single atoms by reversing the thermal sintering process. Atomization of Pt NPs into single atoms makes metal catalytic sites fully exposed and results in engineerable structural and electronic properties, thereby leading to dramatically enhanced enzymatic performance. As expected, the as-prepared thermally stable Pt single-atom nanozyme (Pt_{TS}-SAzyme) exhibited remarkable peroxidase-like catalytic activity and kinetics, far exceeding the Pt nanoparticle nanozyme. The following density functional theory calculations revealed that the engineered P and S atoms not only promote the atomization process from Pt NPs into Pt_{TS}-SAzyme but also endow single-atom Pt catalytic sites with a unique electronic structure owing to the electron donation of P atoms, as well as the electron acceptance of N and S atoms, which simultaneously contribute to the substantial enhancement of the enzyme-like catalytic performance of Pt_{TS}-SAzyme. This work demonstrates that thermal atomization of the metal nanoparticle-based nanozymes into single-atom nanozymes is an effective strategy for engineering high-performance nanozymes, which opens up a new way to rationally design and optimize artificial enzymes to mimic natural enzymes.
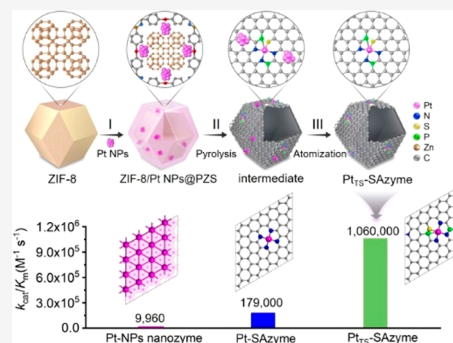
1. INTRODUCTION

Nanozymes are generally defined as nanomaterials with intrinsic enzyme-like properties that have attracted significant interest owing to their capability to address the limitations of traditional enzymes such as high costs in preparation, easy denaturation, and limited practical applications.[1−3] Although great progress has been made in nanozyme engineering, the activities of these nanozymes are much lower than those of natural enzymes.[4,5] In recent years, with the rapid development of nanoscience and nanotechnology, the emerging single-atom catalysts (SACs) featuring isolated metal atoms as active centers have exhibited excellent performance for a wide variety of catalytic reactions.[6−13] Very recently, by mimicking the highly evolved catalytic center of natural enzymes, SACs with well-defined electronic and geometric structures have shown promise to serve as direct surrogates of traditional enzymes.[14−17] However, common approaches to the preparation of these single-atom nanozymes (SAzymes) often lack appropriate interactions between the metal active atoms and supports, resulting in the instability and leaching of active species.[18−20] In particular, due to the high specific surface free energy, single metal atoms have a strong tendency to migrate and aggregate into particles, known as sintering, which leads to the decline and even deactivation of the catalytic performance of SAzymes.[21−23] If we can reverse the sintering process to convert nanoparticles into single atoms via thermal atomization at high temperature, it will allow the formation of thermally stable single-atom materials with single-atom active species anchored at thermodynamically stable sites, which will improve the stability and prevent aggregation and leaching of single-atom active species.[24−29] Additionally, the transformation from nanoparticle-based nanozymes into SAzymes can make metal species fully exposed and enhance the accessibility of active sites,[30−33] which is beneficial for the enhancement of enzymatic performance.[34,35] Therefore, converting nanoparticle-based nanozymes into SAzymes to access stable and active SAzymes is highly desired for engineering high-performance artificial enzymes.

In this work, we achieve for the first time the direct transformation of platinum nanoparticles (Pt NPs) into single atoms to synthesize a thermally stable Pt single-atom nanozyme (Pt_{TS}-SAzyme) via reversing the sintering process. The thermal atomization of Pt NPs into single atoms results in

an engineerable atomic and electronic structure with a unique Pt_1-N_3PS active moiety, which endows Pt_{TS}-SAzyme with remarkable enhancement in peroxidase-like catalytic activity and kinetics. Therefore, direct thermal transformation of metal nanoparticle-based nanozymes into SAzymes is a novel and effective strategy for engineering high-performance nanozymes and provides a stable and practical model for nanozyme study.

2. RESULTS AND DISCUSSION

The schematic preparation process of Pt_{TS}-SAzyme via reversing the sintering to transform Pt NPs into Pt single atoms is displayed in Figure 1a. The Pt NPs with uniform sizes
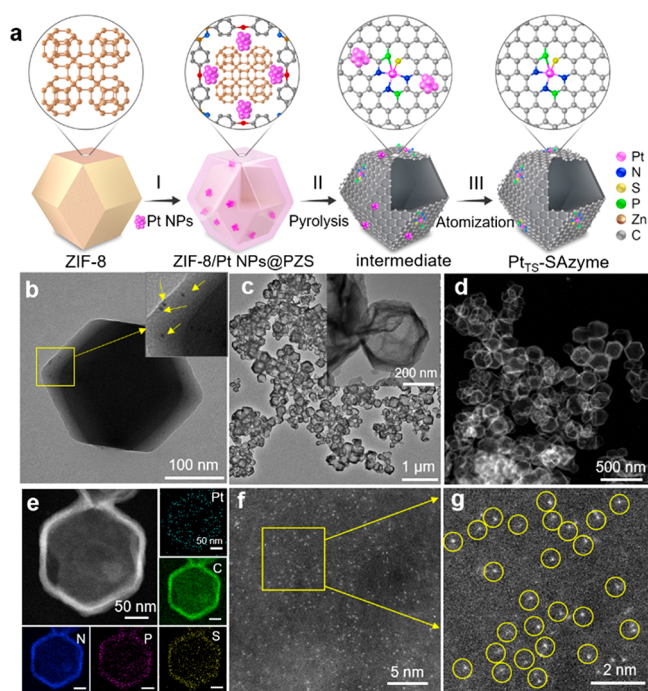

Figure 1. Synthesis and structural characterizations of Pt_{TS}-SAzyme. (a) Illustration of the preparation process of Pt_{TS}-SAzyme. (b) TEM image of ZIF-8/Pt NPs@PZS. (c) TEM and enlarged TEM image (inset), (d) HAADF-STEM, and (e) the corresponding EDS mapping images of Pt_{TS}-SAzyme; the scale bars are 50 nm. (f) AC HAADF-STEM image and (g) an enlarged image of Pt_{TS}-SAzyme.

were prepared (Figure S1) and then supported on the surface of zeolitic imidazolate frameworks (ZIF-8),[36,37] followed by the coating of a poly(cyclotriphosphazene-co-4,4′-sulfonyldiphenol) (PZS) layer to give the ZIF-8/Pt NPs@PZS sandwich structure. As shown in Figure 1b, the transmission electron microscopy (TEM) image of ZIF-8/Pt NPs@PZS displays that Pt NPs are confined in the interlayer of ZIF-8 and PZS, as further confirmed by high-angle annular dark field scanning TEM (HAADF-STEM) imaging (Figures S2 and S3). Energy-dispersive spectroscopy (EDS) mapping measurement demonstrates that C, N, P, and S elements are uniformly dispersed on the entire coating layer of ZIF-8/Pt NPs@PZS (Figure S4), suggesting ZIF-8 is fully wrapped by a PZS layer. Then the ZIF-8/Pt NPs@PZS was pyrolyzed at 1050 °C for 5 h in a flowing N_2 atmosphere. During the pyrolysis process, the Pt NPs gradually disappeared and the substrate of ZIF-8/Pt NPs@PZS transformed into a uniform N, P, S, and Pt co-doped hollow carbon polyhedron (Figure 1c−e). Further observation in the enlarged HAADF-STEM image demon-

strates the absence of Pt clusters (Figure 1c,d). In addition, no Pt characteristic peaks are detected in the pyrolyzed sample of the X-ray diffraction (XRD) pattern (Figure S5), and the signals indexed to Pt species are observed in EDS mapping analysis (Figure 1e), showing the uniform distribution of Pt species over the whole N, P, and S co-doped hollow carbon polyhedron architecture. Inductively coupled plasma optical emission spectrometry (ICP-OES) analysis further determined the Pt content is 0.07 wt %. Moreover, the aberration-corrected HAADF-STEM (AC HAADF-STEM) with atomic resolution measurement was further carried out to investigate the pyrolyzed sample at the atomic scale. As shown in Figure 1f and g, the bright dots associated with Pt atoms are atomically dispersed on the N, P, and S co-doped hollow carbon substrate, suggesting Pt NPs are converted into Pt single atoms via the reversion of sintering to give the final Pt_{TS}-SAzyme.

To understand the atomization process from Pt NPs into single atoms, we performed AC HAADF-STEM measurement to observe the pyrolyzed sample at 1050 °C at different times. As shown in Figure S6, the average size of Pt NPs gradually becomes smaller, the number of Pt NPs gradually becomes less, and the number of Pt single atoms gradually becomes more as the pyrolysis time is prolonged from 1 h to 5 h. This result suggests Pt NPs collide with a N, P, and S co-doped carbon substrate, gradually become smaller, and finally transform to single atoms. The high temperature is critical to provide sufficient activation energy for atom diffusion and to overcome the energy barrier for breaking the Pt−Pt bond in Pt nanoparticles to create Pt single atoms. As shown in Figure S7, when the sample was pyrolyzed at 950 °C for 5 h, the Pt nanoparticles and single atoms coexisted in the pyrolyzed sample, suggesting a lower temperature fails to fully disperse Pt nanoparticles into single atoms. To investigate the effect of ultrahigh temperature (above 1100 °C), in situ environmental transmission electron microscopy (ETEM) was performed. As shown in Figure S8, the representative images obtained at 1100, 1150, and 1200 °C demonstrate that Pt single atoms reaggregate into Pt particles and the particles gradually become larger as the temperature rises. Meanwhile, the N, P, and S co-doped carbon substrate gradually becomes thinner and is even damaged and collapses, because C, N, P, and S elements begin to decompose at the ultrahigh temperature (above 1100 °C), which leads to too few coordination sites to anchor single Pt atoms, thereby leading to the agglomeration of Pt species. Therefore, 1050 °C is the optimal temperature for the thermal atomization of Pt NPs into Pt single atoms.

To investigate the chemical state of C, N, P, and S elements in Pt_{TS}-SAzyme, X-ray photoelectron spectroscopy (XPS) analysis was carried out. The C 1s spectrum shown in Figure S9 exhibits four peaks, associated with graphitic C=C (284.8 eV), C−N (288.3 eV), C−P (285.6 eV), and C−S (284.5 eV). The N 1s spectrum as displayed in Figure S10 can be deconvoluted into five peaks at binding energies of 398.3, 400.2, 401.3, 403.6, and 399.2 eV, which are attributed to pyridinic N, pyrrolic N, graphitic N, pyridinic N^+-O^-, and Pt−N. The fitting result of the P 2p spectrum shows the coexistence of the P−C peak at the binding energy of 132.7 eV and P−O peak at the binding energy of 134.2 eV (Figure S11). The S 2p spectrum matches well with the superposition of the peak ascribed to the oxidized S (168.8 eV) and the peaks from $2p_{3/2}$, $2p_{1/2}$ splitting of the S 2p spin orbital (−C−S−C−) at the binding energy of 164.2 and 165.4 eV (Figure S12).

To further investigate the chemical states and local structure of the Pt_{TS}-SAzyme, structure-sensitive XAFS measurements were carried out. Figure 2a displays the Fourier transformed
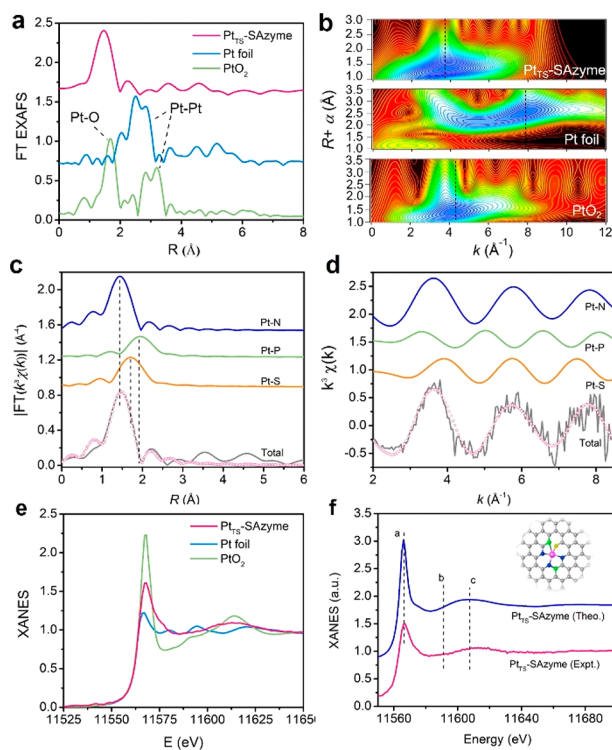

Figure 2. Atomic structural analysis of Pt_{TS}-SAzyme. (a) Fourier-transformed magnitudes of the experimental Pt L_3-edge EXAFS signals of Pt_{TS}-SAzyme, Pt foil, and PtO_2. (b) WT curves of Pt_{TS}-SAzyme, Pt foil, and PtO_2. (c) EXAFS fitting analysis of Pt_{TS}-SAzyme in R space. Curves from top to bottom are the Pt−N, Pt−P, and Pt−S three-body backscattering signals, the fitting curve total signal (pink line), and the experimental signal (gray line). (d) EXAFS fitting analysis of Pt_{TS}-SAzyme in k space. (e) Pt L_3-edge XANES spectra of Pt_{TS}-SAzyme, Pt foil, and PtO_2. (f) Comparison between the experimental XANES spectra (pink line) and theoretically simulated XANES spectra (blue line) of Pt_{TS}-SAzyme.

(FT) extended Pt L-edge X-ray absorption fine structure (EXAFS) spectra of Pt_{TS}-SAzyme, which exhibits a main peak at about 1.5 Å, close to the Pt−O peak in PtO, which suggests that this peak is associated with the backscattering between Pt and light atoms. Unlike Pt foil, no obvious peak at about 2.5 Å ascribed to Pt−Pt coordination is detected in Pt_{TS}-SAzyme, which excludes the formation of metallic crystalline Pt species and confirms the sole existence of isolated single Pt atoms, consistent with AC HAADF-STEM results. Furthermore, EXAFS wavelet transform (WT) analysis was performed, which is a powerful tool to discriminate the backscattering atoms even though they overlap substantially in R space. As shown in Figure 2b, only one intensity maximum at about 3.8 Å^{-1} was detected in the WT contour plot of Pt_{TS}-SAzyme, indexed to the coordination contribution between Pt and light atoms, consistent with the analysis result of the WT contour plot of PtO_2. In comparison to Pt foil, there is no intensity maximum at 7.9 Å^{-1} associated with the Pt−Pt contribution in the WT contour plot of Pt_{TS}-SAzyme, further confirming that Pt species in the Pt_{TS}-SAzyme are atomically dispersed without the existence of metal-derived crystalline structures.

Quantitative least-squares EXAFS curve-fitting analysis was carried out to extract the coordination configurations of the active center of Pt_{TS}-SAzyme. As shown in Figure 2c and d, the best-fitting results demonstrate that the dominant peak around 1.5 Å is ascribed to the overlap of Pt−N Pt−P, and Pt−S first-shell coordination (Table S1). For comparison, the fitting analyses of Pt foil and PtO_2 were also performed and are shown in Figures S13 and S14. X-ray absorption near edges structure (XANES) spectra are sensitive to the three-dimensional arrangement of atoms around the center metal, which can serve as a powerful tool to identify the atomic configuration. Figure 2e displays the Pt L_3-edge XANES curves, where the absorption edge of Pt_{TS}-SAzyme is between that of Pt foil and PtO_2, indicating atomically dispersed Pt species carry a positive charge. Moreover, the XANES theoretical calculation was performed, which shows that the XANES profile of Pt_{TS}-SAzyme can be well reproduced by the Pt_1-N_3PS moiety from quantitative EXAFS curve-fitting analysis (Figure 2f), suggesting a porphyrin-based Pt_1-N_3PS moiety of Pt_{TS}-SAzyme, as schematically displayed in the inset of Figure 2f.

Pt NPs with intrinsic peroxidase-like catalytic activity attract significant current interest due to their ability to replace specific peroxidase enzymes in peroxidase-based applications.[38−41] As shown in Figure 3a, a Pt-NPs nanozyme with Pt NPs supported on a N, P, and S co-doped hollow carbon polyhedron was prepared (Figure S15), which exhibits intrinsic peroxidase-like activity by catalyzing the oxidation of peroxidase substrates (e.g., 3,3′,5,5′-tetramethylbenzidine (TMB), diazoaminobenzene (DAB), or o-phenylenediamine (OPD)) to produce colorimetric reactions. After thermal atomization of Pt NPs into single atoms, the peroxidase-like catalytic activity of Pt active sites was significantly increased from 1.05 units to 21.8 units (U, one activity unit is defined as the amount of nanozyme that catalyzes 1 μmol of product per minute[42]) per nmol of Pt atoms (Figure 3b,c). The dynamic light scattering (DLS) measurements were carried out to investigate the diameter distribution of Pt_{TS}-SAzyme and Pt-NPs nanozyme. As shown in Figure S16, the diameter of Pt_{TS}-SAzyme via DLS analysis is about 158.6 nm. The diameter of Pt-NPs nanozyme via DLS analysis is about 165.3 nm (Figure S17). The small polydispersity index (PDI) of Pt_{TS}-SAzyme and Pt-NPs nanozyme indicates a high uniformity in the sizes. The pure support of a N, P, and S co-doped hollow carbon polyhedron (NPS-HC) without Pt active sites was also prepared (Figure S18), which exhibits little peroxidase-like catalytic activity (Figure 3b). We further quantitatively characterized the catalytic kinetics of Pt-NPs nanozyme and Pt_{TS}-SAzyme, respectively, by plotting the initial reaction velocity against the varied substrate concentrations (Figure 3d). The thermally atomized Pt_{TS}-SAzyme catalyzes the oxidation of peroxidase substrates according to Michaelis−Menten kinetics and shows a significantly higher catalytic rate constant (k_{cat} = 329 s^{-1}) and catalytic efficiency (k_{cat}/K_m = 1.06 × 10^6 M^{-1} s^{-1}) than that of the Pt-NPs nanozyme (k_{cat} = 8.67 s^{-1}; k_{cat}/K_m = 9.96 × 10^3 M^{-1} s^{-1}) (Table S3). In addition, Pt_{TS}-SAzyme shows an optimum catalytic activity under a wide range of temperatures (30−60 °C), and the optimal pH is approximately pH 4.3 (Figure S19). Moreover, Pt_{TS}-SAzyme exhibits a high storage stability, and no activity decrease was observed after 2 weeks of storage at 25 °C (Figure S20).
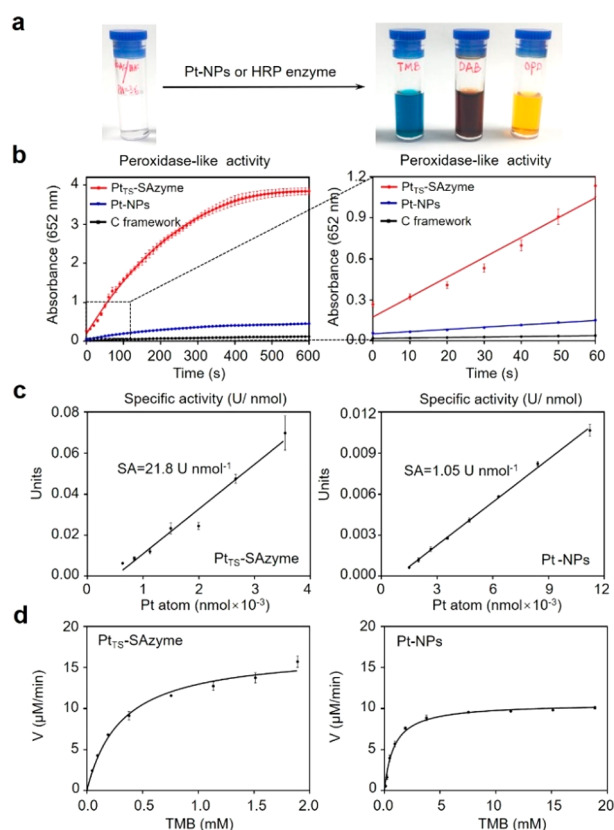
C

Figure 3. Peroxidase-like catalytic activity characterization of Pt$_{TS}$-SAzyme. (a) Pt-based nanozymes show the intrinsic peroxidase-like activity and catalyze the oxidation of peroxidase substrates (TMB, DAB, and OPD) to produce colorimetric reactions. (b) Left, reaction−time curves of TMB colorimetric reaction catalyzed by Pt$_{TS}$-SAzyme, Pt-NPs nanozyme, or the inorganic C framework (NPS-HC) without Pt active sites. Right, the magnified initial linear portion of the reaction−time curves. A length of 60 s was chosen for the initial rate period because the R^2 coefficients were close to 1 during this period after a linear-regression analysis. Absorbance measured in arbitrary units. (c) Specific activities (U/nmol Pt atoms) of Pt$_{TS}$-SAzyme and Pt-NPs nanozyme. (d) Catalytic kinetics of Pt$_{TS}$-SAzyme and Pt-NPs nanozyme. The initial reaction velocity (v) was measured in 0.2 M NaAc/HAc buffer pH 3.6 at 37 °C. The concentration of H$_2$O$_2$ was 1.0 M, and the TMB concentrations was varied (n = 3 independent measurements, error bars represent mean ± SD).

Meanwhile, Pt$_{TS}$-SAzyme also exhibited superior catalytic performance when compared with previously reported Pt-based nanozymes,[1−5] further confirming the catalytic advantages of Pt$_{TS}$-SAzyme. The results suggest that thermal atomization of Pt NPs into single atoms can be an effective strategy for engineering high-performance nanozymes.

We further performed density functional theory (DFT) calculations to understand the catalytic reaction mechanism and shed light on the dramatically improved catalytic performance of Pt$_{TS}$-SAzyme after thermal atomization from Pt NPs. We first demonstrated the atomization process from the Pt$_{10}$ cluster to PtN$_3$PS and PtN$_4$ single atoms, in which PtN$_3$PS and PtN$_4$ represent two kinds of Pt single-atom nanozymes with different coordination of N, P, and S atoms. As shown in Figure 4a, the single Pt atom formation of PtN$_3$PS and PtN$_4$ from Pt$_{10}$ cluster decomposition needs to overcome a very high barrier of 1.98 and 2.46 eV, but with a large exothermicity of 1.91 and 3.53 eV, suggesting the Pt single

atom is much more stable than the Pt cluster thermodynamically and the existence of P and S elements can promote the thermal atomization from Pt NPs to single atoms (1.98 vs 2.46 eV); however the atomization process needs to be accomplished at a very high temperature, which is well in agreement with the thermal atomization process performed at 1050 °C. The DFT calculation results and experimental results together well suggest that Pt atoms are gradually stripped from the surface of Pt NPs driven by high temperature and then are trapped by anchoring sites of a N, P, and S co-doped carbon substrate to form thermally stable Pt single atoms.

Subsequently, to understand the origin of the high peroxidase-like catalytic performance of Pt$_{TS}$-SAzyme, we compared the adsorptions of the reactants (H$_2$O$_2$ and TMB, in which TMB is used as the peroxidase substrate and H$_2$O$_2$ as the oxidant) on the different Pt active centers thermodynamically. Based on the characterized atomic structure of the Pt active sites anchored by the richly doped P and S atoms of Pt$_{TS}$-SAzyme (Figure 2), as well as the DFT comparison of the total energies of different P, S double-doped structures (Figure S21), three catalyst models of PtN$_3$PS, PtN$_4$, and Pt(111) were constructed in the calculations (their top and side view structures are shown in Figure S22), in which Pt-NPs nanozyme with a Pt(111) surface was used to compare with the two kinds of Pt single-atom nanozymes with an active PtN$_3$PS moiety and active PtN$_4$ moiety. As show in Figure 4b, the adsorption energies of H$_2$O$_2$ and TMB are close on the front and reverse sides of PtN$_3$PS (−0.20 to −0.30 eV), indicating both H$_2$O$_2$ and TMB exhibit weak physical adsorption and that they are competitive. For comparison, the adsorption of H$_2$O$_2$ is more favorable than that of TMB on the PtN$_4$ (−0.22 vs −0.01 eV), suggesting the TMB adsorption is uncompetitive. However, it is clear that the adsorption of TMB is much more favorable than that of H$_2$O$_2$ (−2.02 vs −0.30 eV) on the Pt(111), revealing that the TMB is hardly desorbed from the surface of the Pt cluster because of the very strong adsorption, which probably leads to catalyst poisoning.

Meanwhile, in view of the fact that the peroxidase substrates can be oxidized by the free radicals, we also performed the mechanisms of H$_2$O$_2$ reduction forming surface OH or O species dynamically. In Figure S23, all the possible routes of H$_2$O$_2$ dissociation into the surface O species are studied on the three catalyst models of PtN$_3$PS, PtN$_4$, and Pt(111), and the most favorable pathways for the oxidation of TMB by the surface O species at neutral conditions are displayed in Figure 4c. Moreover, the effect of acidic media on the oxidation of TMB is carried out as well (Figure S24), in which the reaction of OH + H → H$_2$O, as well as the oxidation of TMB by the surface OH species from H$_2$O$_2$ dissociation, is investigated.

As shown in Figure 4c, all of the H$_2$O$_2$ cannot be adsorbed on the three catalysts of PtN$_3$PS, PtN$_4$, and Pt(111); their adsorption energies are −0.20, −0.22, and −0.30 eV, respectively. Then, the floating H$_2$O$_2$ will be dissociated into two surface OH species (H$_2$O$_2$ → 2OH) with barriers of 0.93 and 0.35 eV on the models of PtN$_3$PS and Pt(111), while it is hardly decomposed on the PtN$_4$ because of the very high barrier (1.95 eV). Surprisingly, the two surface species of OH are adsorbed simultaneously on the P atom doped in PtN$_3$PS, while they are adsorbed on the Pt atom in PtN$_4$ and Pt(111) models. After that, only on the Pt(111) surface can the two surface OH species react easily with each other, forming the surface O species and a floating H$_2$O molecule (2OH → O + H$_2$O) with a very low barrier of 0.10 eV. However, a similar
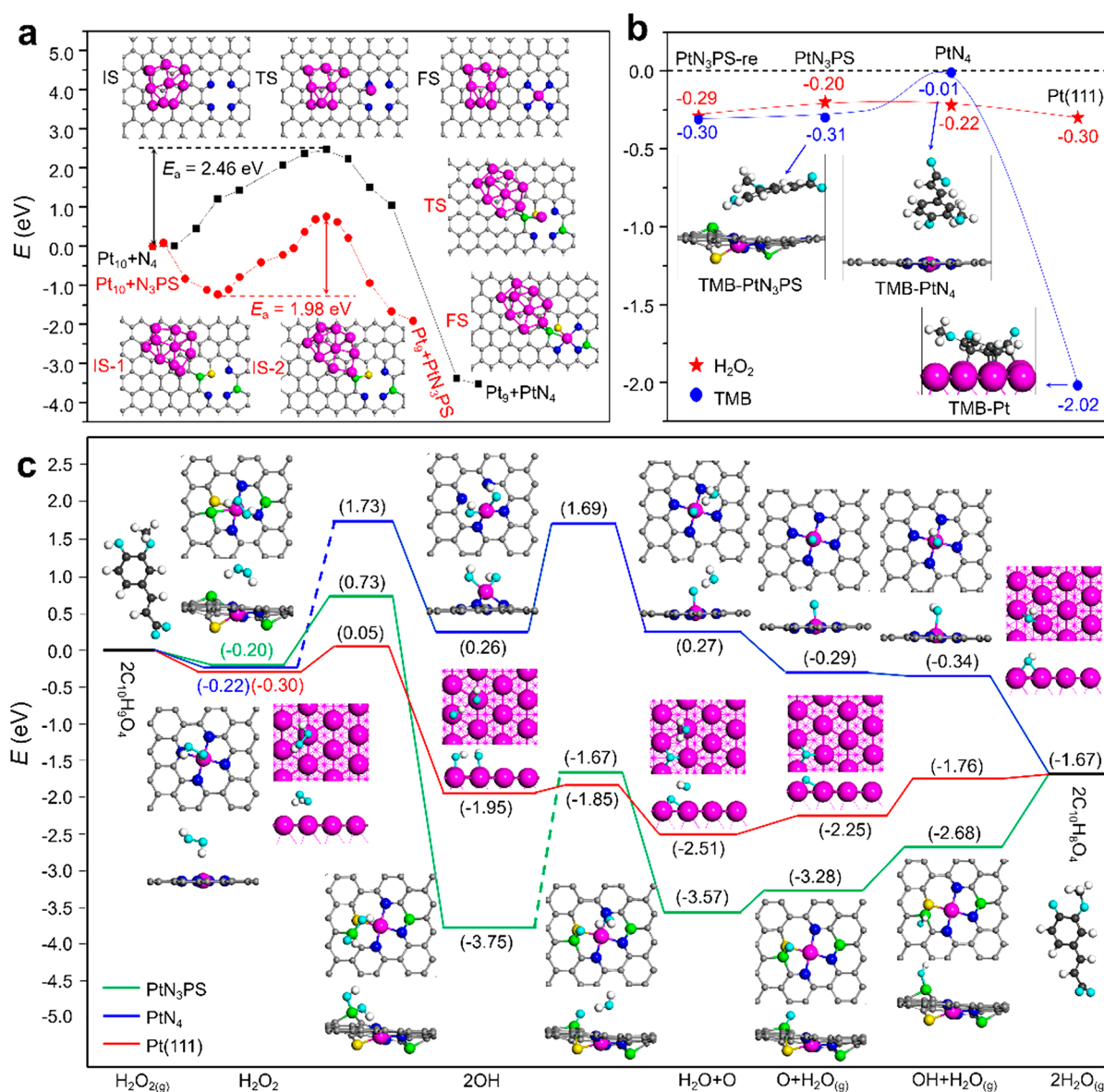
Figure 4. DFT studies on the catalytic reaction mechanism of PtN₃PS-SAzyme. (a) Thermal atomization process of a Pt₁₀ cluster to PtN₃PS and PtN₄ single atoms. (b) Thermodynamic adsorptions of H_2O_2 and TMB on PtN₃PS-SAzyme, PtN₄-SAzyme, and Pt-NPs nanozyme. (c) Peroxidase-like activity of the three models. In the energy profiles, the most favorable paths of H_2O_2 dissociation into surface O species, as well as the oxidation reaction of TMB in the thermodynamics, are shown. The Pt, C, N, P, S, O, and H atoms are given in pink, gray, blue, green, yellow, cyan, and white, respectively, while in order to make a distinction, the C atoms in TMB are shown in dark gray.

reaction can hardly occur because of the very high barriers of 2.08 and 1.43 eV on the PtN₃PS and PtN₄ models. In addition, the H_2O desorption and the TMB oxidation by the surface O species are explored. The calculation results show that the H_2O can be desorbed easily on PtN₃PS, PtN₄, and Pt(111) with reaction energies of 0.29, 0.26, and −0.56 eV, respectively; the TMB also can be oxidized by the surface O and OH species with reaction energies of 1.01, 0.09, and −1.33 eV.

In the acidic media (Figure S24), the calculations reveal that the H atom still can be strongly adsorbed on PtN₃PS, PtN₄, and Pt(111), even if there have been two surface species of OH from H_2O_2 dissociation, forming the structures of 2OH + H, in which the atomic H is located at the top site of the Pt atom in PtN₃PS and Pt(111), while it is located at the top site of atomic N in PtN₄. Starting with 2OH + H, the reaction of 2OH + H → OH + H_2O has barriers of 1.44, 0.96, and 0.36

eV, respectively, on the three models of PtN₃PS, PtN₄, and Pt(111), reflecting that the acidic media has little effect on the single-atom Pt catalysts of PtN₃PS and PtN₄, but it will give rise to the prompt transformation of surface OH species into H_2O, leading to the interruption of the catalytic cycle.

Clearly, the PtN₃PS single-atom nanozyme with an active PtN₃PS moiety possesses a more outstanding enzymatic performance compared with PtN₄ and Pt(111). Thermodynamically, the adsorption of H_2O_2 and TMB is competitive on PtN₃PS, which simultaneously favors the H_2O_2 decomposition and TMB oxidation. Dynamically, not only can the PtN₃PS dissociate H_2O_2 into two surface OH species (H_2O_2 → 2OH, 0.93 eV), but also the OH species can further oxidize TMB with a matched barrier of 1.01 eV. Unfortunately, the surface OH species cannot be converted into O species via the disproportionation reaction (2OH → O + H_2O, 2.08 eV),
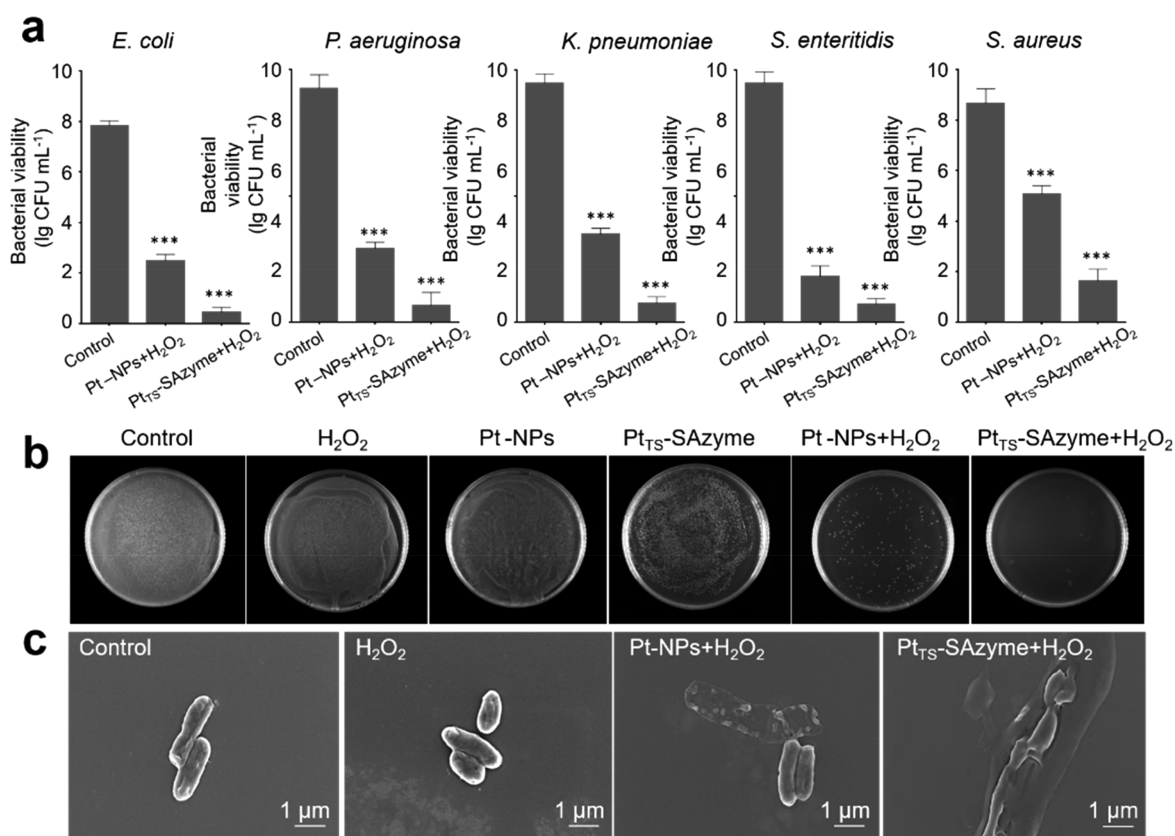
Figure 5. Antibacterial effect of Pt_{TS}-SAzyme. (a) Comparison of the antibacterial effects of Pt_{TS}-SAzyme (0.25 mg/mL) and Pt-NPs nanozyme (0.25 mg/mL) against *E. coli*, *P. aeruginosa*, *S. enteritidis*, *K. pneumoniae*, and *S. aureus* in the presence of H_2O_2 (1 mM). (b) Representative colony formation of *E. coli* in different treatment groups. (c) Representative SEM images of *E. coli* treated by Pt_{TS}-SAzyme (0.25 mg/mL) or Pt-NPs nanozyme (0.25 mg/mL) in the presence of H_2O_2 (1 mM). Data are represented as the mean ± SD. All experiments were performed in triplicate. Statistical significance was assessed using an unpaired Student's two-sided *t* test compared to the control group. ***$p < 0.001$.

which could not further promote the enzymatic performance. For the Pt single-atom nanozyme with active PtN_4 moiety, although TMB can be oxidized by either OH or O species, the H_2O_2 cannot be dissociated into surface OH or O species (1.95 and 1.43 eV), leading to the lower catalytic activity of the PtN_4 single-atom nanozyme. For the Pt(111) surface, although the H_2O_2 can be dissociated easily into surface OH and/or O species (0.35 and 0.10 eV), the strong adsorption of TMB (−2.02 eV) will lead to catalyst poisoning, and the acidic media also can give rise to the failure of the whole catalytic process.

Furthermore, to investigate the modulation of the local atomic configuration and electronic structure of the central Pt atoms by the coordinated P and S atoms, the inverse Bader charge (Figure S25a) of different kinds of atoms in PtN_3PS and PtN_4, the charge density differences (Figure S25b and c) of Pt atom in PtN_3PS and PtN_4, the charge density differences (Figure S25d) of the top-layer Pt atoms in Pt(111), and the charge density differences (Figure S25e−g) of P and S atoms in PtN_3PS are analyzed. To avoid misunderstanding, the inverse Bader charge is given here, which can be seen as the charge of the different atoms. For PtN_4, the charge of the Pt atom is +0.76, and the average charge of the four N and C atoms is −1.14 and +0.06, indicating the Pt atom and graphitic layer would donate electrons to the doped N atoms. For the catalyst of PtN_3PS, the average charge of the P atom is +1.41, the charge of the S atom is −0.13, the charge of the Pt atom is lower than that in PtN_4 (+0.59 vs +0.76), and the average

charge of N (−1.21 vs −1.14) and C (+0.02 vs +0.06) atoms in the graphitic layer is slightly higher and lower than that in the PtN_4, respectively. The results show that the doped P atom could intensively donate electron to the Pt atom and C atoms of the graphitic layer, while the doped S atom is the opposite, which could slightly accept electrons from the Pt and graphitic layer. In total, the charge of the metal center Pt ($Pt^{\delta+}$) becomes less positive, which agrees with the XANES results in our experiment, as well as the corresponding analysis of the charge density difference. For comparison, the charge density differences (Figure S25d) of the top-layer Pt atoms in Pt(111) are analyzed as well, and the electron accumulation and depletion areas at the inside and outside of the top Pt layer can be clearly found, which gives rise to the very strong adsorption of TMB on the hollow sites of Pt nanoparticles. Therefore, based on the analysis of the electronic properties of these three catalysts, it is inferred that the electron donation of the P atom and electron acceptation of N and S atoms leads to the unique electronic space structure of PtN_3PS and further enhances the catalytic activity. In other words, the high catalytic activity of PtN_3PS contributes the synergistic effects of Pt, N, P, and S atoms.

To demonstrate the unique properties of the thermally stable single-atom enzyme that is synthesized by the atomization process from nanoparticles, an ordinary Pt single-atom enzyme (Pt-SAzyme) was prepared by the common route for the synthesis of a single-atom catalyst, which undergoes the absorption of the mononuclear metal

precursor, followed by reduction and stabilization on N, P, and S co-doped hollow carbon (see details in the experimental section of the Supporting Information and Figures S26 and S27). As shown in Figure S28, Pt atoms are atomically dispersed in the Pt-SAzyme. The XAFS analysis and the quantitative least-squares EXAFS curve-fitting analysis of Pt-SAzyme demonstrate that Pt species of Pt-SAzyme exist in the form of isolated Pt single atoms with the Pt_1-N_4 active moiety (Figures S29, S30 and Table S2), which is distinguished from the Pt_{TS}-SAzyme with the Pt_1-N_3PS active moiety. The above results reveal that the geometrical and electronic structure of active sites in Pt_{TS}-SAzyme synthesized by the thermal atomization process from nanoparticles is different from that in Pt-SAzyme synthesized by a common route. Furthermore, we compared the enzyme performance of Pt_{TS}-SAzyme and Pt-SAzyme (Figure S31 and Table S3). It can be seen that Pt_{TS}-SAzyme exhibits a peroxidase-like activity of 21.8 U/nmol Pt atom, which is much higher than that of Pt-SAzyme (4.19 U/nmol Pt atom), and the k_{cat}/K_m of Pt_{TS}-SAzyme is 1.06×10^6 M^{-1} s^{-1}, which is 5.9 times as high as that of Pt-SAzyme (1.79×10^5 M^{-1} s^{-1}), suggesting better catalytic kinetics of Pt_{TS}-SAzyme. These experimental results are in good agreement with the DFT calculation, which demonstrates that the unique structure of Pt_{TS}-SAzyme with synergistic N, P, and S coordination with atomically dipsersed Pt atoms contributes to the remarkable performance.

Peroxidase-like nanozymes have been widely developed for antibacterial application by employing their peroxidase-like catalytic activity to decompose H_2O_2 into highly toxic free radicals that disrupt the bacterial membrane and induce bacterial apoptosis.[43−46] We further evaluated the antibacterial effects of Pt_{TS}-SAzyme and Pt-NPs nanozyme against five representative bacteria: Gram-negative *Escherichia coli* (*E. coli*), *Pseudomonas aeruginosa* (*P. aeruginosa*), *Salmonella enteritidis* (*S. enteritidis*), and *Klebsiella pneumoniae* (*K. pneumoniae*) and Gram-positive *Staphylococcus aureus* (*S. aureus*). In the presence of H_2O_2 (1 mM), Pt_{TS}-SAzyme (0.25 mg/mL) shows high antibacterial effects on these five bacteria with an inhibition rate of ≥90% against *E. coli*, *P. aeruginosa*, *S. enteritidis*, and *K. pneumoniae* and an inhibition rate of 81% on *S. aureus* (Figure 5a,b). In comparison, Pt-NPs nanozyme (0.25 mg/mL) exhibits a much lower antibacterial activity than that of Pt_{TS}-SAzyme (Figure 5a,b) under the same experimental conditions, indicating the significantly improved antibacterial activity of Pt_{TS}-SAzyme after thermal atomization from Pt-NPs nanozyme. In comparison with other nanozymes used for antibacterial activity, Pt_{TS}-SAzyme shows a broad sterilization spectrum and a high efficiency (see details in Table S4). The bacterial morphology of the treated bacteria in different groups was further characterized by scanning electron microscopy (SEM). As shown in Figure 5c, the morphology and structural integrity of *E. coli* are severely affected after being treated with Pt_{TS}-SAzyme (0.25 mg/mL) in the presence of H_2O_2 (1 mM), whereas the group cultured with H_2O_2 (1 mM) only shows a negligible antibacterial effect. Thus, the results reveal that the thermally atomized Pt_{TS}-SAzyme from Pt-NPs nanozyme exhibits a remarkable peroxidase-like catalytic activity and induces a highly effective bacterial lethality.

H_2O_2 is the most common disinfectant used to destroy the active components of bacteria, such as cell membranes, proteins, and nucleic acids.[47−49] However, drug resistance is easy to develop due to the low efficiency and high concentration of H_2O_2 (2 M) required during antibacterial applications in the clinic.[50] The results reveal that a small amount of Pt_{TS}-SAzyme (0.25 mg/mL) can kill ≥90% of *E. coli* with a low concentration of H_2O_2 (1 mM), while the sterilization efficiency is negligible without the addition of Pt_{TS}-SAzyme (Figure 5a,b). Therefore, developing high-performance nanozyme-based antibiotics provides a new strategy for the solving of bacterial infection and bacterial resistance.

3. CONCLUSIONS

In summary, for the first time we report the direct transformation of Pt NPs into Pt single atoms to obtain a high-performance Pt single-atom nanozyme (Pt_{TS}-SAzyme) via reversing the sintering process. The as-prepared Pt_{TS}-SAzyme exhibits an outstanding peroxidase-like activity and kinetics, which is much higher than those of Pt-NPs nanozyme. AC HAADF-STEM and XAFS characterizations as well as DFT calculations demonstrate the synergistic effects of Pt, N, P, and S atoms for the unique Pt_1-N_3PS active moiety of Pt_{TS}-SAzyme contribute to the remarkable catalytic activity and kinetics. This work presents that the thermal atomization of metal NPs-based nanozymes into SAzymes is an effective strategy to enhance their enzymatic performance, thus providing a new method for the design and engineering of high-performance artificial enzymes to promote alternatives for natural enzymes.

■ ASSOCIATED CONTENT

ⓈI Supporting Information

The Supporting Information is available free of charge at https://pubs.acs.org/doi/10.1021/jacs.1c08581.

Detailed experimental procedures, characterization methods, extended figures, and tables (PDF)

■ AUTHOR INFORMATION

Corresponding Authors

Minmin Liang − *Experimental Center of Advanced Materials, School of Materials Science & Engineering, Beijing Institute of Technology, Beijing 100081, China;* ⓞ orcid.org/0000-0002-5152-5240; Email: mmliang@bit.edu.cn

Dingsheng Wang − *Department of Chemistry, Tsinghua University, Beijing 100084, China;* ⓞ orcid.org/0000-0003-0074-7633; Email: wangdingsheng@mail.tsinghua.edu.cn

Authors

Yuanjun Chen − *Department of Chemistry, Tsinghua University, Beijing 100084, China*

Peixia Wang − *Institute of Molecular Medicine, College of Future Technology and Peking-Tsinghua Center for Life Sciences, Peking University, Beijing 100871, China*

Haigang Hao − *College of Chemistry and Chemical Engineering, Inner Mongolia University, Hohhot 010021, China*

Juanji Hong − *Experimental Center of Advanced Materials, School of Materials Science & Engineering, Beijing Institute of Technology, Beijing 100081, China*

Haijing Li − *Beijing Synchrotron Radiation Facility, Institute of High Energy Physics, Chinese Academy of Sciences, Beijing 100049, China*

Shufang Ji − *Department of Chemistry, Tsinghua University, Beijing 100084, China*

Ang Li − *Beijing Key Laboratory of Microstructure and Property of Advanced Materials, Beijing University of Technology, Beijing 100024, China;* ⦿ orcid.org/0000-0002-9802-9359

Rui Gao − *College of Chemistry and Chemical Engineering, Inner Mongolia University, Hohhot 010021, China*

Juncai Dong − *Beijing Synchrotron Radiation Facility, Institute of High Energy Physics, Chinese Academy of Sciences, Beijing 100049, China;* ⦿ orcid.org/0000-0001-8860-093X

Xiaodong Han − *Beijing Key Laboratory of Microstructure and Property of Advanced Materials, Beijing University of Technology, Beijing 100024, China;* ⦿ orcid.org/0000-0002-0193-1291

Yadong Li − *Department of Chemistry, Tsinghua University, Beijing 100084, China;* ⦿ orcid.org/0000-0003-1544-1127

Complete contact information is available at:
https://pubs.acs.org/10.1021/jacs.1c08581

Author Contributions
[‡]Y.C., P.W., H.H., and J.H. contributed equally to this work.

Notes
The authors declare no competing financial interest.

REFERENCES

(1) Wu, J.; Wang, X.; Wang, Q.; Lou, Z.; Li, S.; Zhu, Y.; Qin, L.; Wei, H. Nanomaterials with enzyme-like characteristics (nanozymes): next-generation artificial enzymes (II). *Chem. Soc. Rev.* **2019**, *48*, 1004−1076.

(2) Huang, Y.; Ren, J.; Qu, X. Nanozymes: classification, catalytic mechanisms, activity regulation, and applications. *Chem. Rev.* **2019**, *119*, 4357−4412.

(3) Fan, K.; Cao, C.; Pan, Y.; Lu, D.; Yang, D.; Feng, J.; Song, L.; Liang, M.; Yan, X. Magnetoferritin nanoparticles for targeting and visualizing tumour tissues. *Nat. Nanotechnol.* **2012**, *7*, 459−464.

(4) Liang, M.; Yan, X. Nanozymes: from new concepts, mechanisms, and standards to applications. *Acc. Chem. Res.* **2019**, *52*, 2190−2200.

(5) Wang, Q. Q.; Wei, H.; Zhang, Z. Q.; Wang, E. K.; Dong, S. J. Nanozyme: An emerging alternative to natural enzyme for biosensing and immunoassay. *TrAC, Trends Anal. Chem.* **2018**, *105*, 218−224.

(6) Cui, X.; Li, W.; Ryabchuk, P.; Junge, K.; Beller, M. Bridging homogeneous and heterogeneous catalysis by heterogeneous single-metal-site catalysts. *Nat. Catal.* **2018**, *1*, 385−397.

(7) Yang, J.; Li, W.; Wang, D.; Li, Y. Single-atom materials: small structures determine macroproperties. *Small Struct.* **2021**, *2*, 2000051.

(8) Cui, T.; Ma, L.; Wang, S.; Ye, C.; Liang, X.; Zhang, Z.; Meng, G.; Zheng, L.; Hu, H.-S.; Zhang, J.; Duan, H.; Wang, D.; Li, Y. Atomically dispersed Pt−N_3C_1 sites enabling efficient and selective electro-catalytic C−C bond cleavage in lignin models under ambient conditions. *J. Am. Chem. Soc.* **2021**, *143*, 9429−9439.

(9) Xiong, Y.; Sun, W.; Han, Y.; Xin, P.; Zheng, X.; Yan, W.; Dong, J.; Zhang, J.; Wang, D.; Li, Y. Cobalt single atom site catalysts with ultrahigh metal loading for enhanced aerobic oxidation of ethylbenzene. *Nano Res.* **2021**, *14*, 2418−2423.

(10) Abdel-Mageed, A. M.; Rungtaweevoranit, B.; Parlinska-Wojtan, M.; Pei, X.; Yaghi, O. M.; Behm, R. J. Highly active and stable single-atom Cu catalysts supported by a metal-organic framework. *J. Am. Chem. Soc.* **2019**, *141*, 5201−5210.

(11) Sun, Q.; Wang, N.; Zhang, T.; Bai, R.; Mayoral, A.; Zhang, P.; Zhang, Q.; Terasaki, O.; Yu, J. Zeolite-Encaged single-atom rhodium catalysts: highly-efficient hydrogen generation and shape-selective tandem hydrogenation of nitroarenes. *Angew. Chem., Int. Ed.* **2019**, *58*, 18570−18576.

(12) Wang, A.; Li, J.; Zhang, T. Heterogeneous single-atom catalysis. *Nat. Rev. Chem.* **2018**, *2*, 65−81.

(13) Hou, C.-C.; Zou, L.; Sun, L.; Zhang, K.; Liu, Z.; Li, Y.; Li, C.; Zou, R.; Yu, J.; Xu, Q. Single-atom iron catalysts on overhang-eave carbon cages for high-performance oxygen reduction reaction. *Angew. Chem., Int. Ed.* **2020**, *59*, 7384−7389.

(14) Huang, L.; Chen, J. X.; Gan, L. F.; Wang, J.; Dong, S. J. Single-atom nanozymes. *Sci. Adv.* **2019**, *5*, eaav5490.

(15) Xiang, H. J.; Feng, W.; Chen, Y. Single-atom catalysts in catalytic biomedicine. *Adv. Mater.* **2020**, *32*, 1905994.

(16) Jiao, L.; Yan, H. Y.; Wu, Y.; Gu, W. L.; Zhu, C. Z.; Du, D.; Lin, Y. H. When nanozymes meet single-atom catalysis. *Angew. Chem., Int. Ed.* **2020**, *59*, 2565−2576.

(17) Wu, W. W.; Huang, L.; Wang, E. K.; Dong, S. J. Atomic engineering of single-atom nanozymes for enzyme-like catalysis. *Chem. Sci.* **2020**, *11*, 9741−9756.

(18) Corma, A.; Concepcion, P.; Boronat, M.; Sabater, M. J.; Navas, J.; Yacaman, M. J.; Larios, E.; Posadas, A.; Lopez-Quintela, M. A.; Buceta, D.; Mendoza, E.; Guilera, G.; Mayoral, A. Exceptional oxidation activity with size-controlled supported gold clusters of low atomicity. *Nat. Chem.* **2013**, *5*, 775−81.

(19) Chen, Y.; Ji, S.; Chen, C.; Peng, Q.; Wang, D.; Li, Y. Single-atom catalysts: synthetic strategies and electrochemical applications. *Joule* **2018**, *2*, 1242−1264.

(20) Kaiser, S. K.; Chen, Z.; Faust Akl, D.; Mitchell, S.; Perez-Ramirez, J. Single-atom catalysts across the periodic table. *Chem. Rev.* **2020**, *120* (21), 11703−11809.

(21) Peter, M.; Flores Camacho, J. M.; Adamovski, S.; Ono, L. K.; Dostert, K. H.; O'Brien, C. P.; Roldan Cuenya, B.; Schauermann, S.; Freund, H. J. Trends in the binding strength of surface species on nanoparticles: how does the adsorption energy scale with the particle size? *Angew. Chem., Int. Ed.* **2013**, *52*, 5175−5179.

(22) Jeong, H.; Kwon, O.; Kim, B.-S.; Bae, J.; Shin, S.; Kim, H.-E.; Kim, J.; Lee, H. Highly durable metal ensemble catalysts with full dispersion for automotive applications beyond single-atom catalysts. *Nat. Catal.* **2020**, *3*, 368−375.

(23) Ji, S.; Chen, Y.; Wang, X.; Zhang, Z.; Wang, D.; Li, Y. Chemical synthesis of single atomic site catalysts. *Chem. Rev.* **2020**, *120*, 11900−11955.

(24) Jones, J.; Xiong, H.; DeLaRiva, A. T.; Peterson, E. J.; Pham, H.; Challa, S. R.; Qi, G.; Oh, S.; Wiebenga, M. H.; Pereira Hernandez, X. I.; Wang, Y.; Datye, A. K. Thermally stable single-atom platinum-on-ceria catalysts via atom trapping. *Science* **2016**, *353*, 150−154.

(25) Moliner, M.; Gabay, J. E.; Kliewer, C. E.; Carr, R. T.; Guzman, J.; Casty, G. L.; Serna, P.; Corma, A. Reversible transformation of pt nanoparticles into single atoms inside high-silica chabazite zeolite. *J. Am. Chem. Soc.* **2016**, *138*, 15743−15750.

(26) Wei, S.; Li, A.; Liu, J. C.; Li, Z.; Chen, W.; Gong, Y.; Zhang, Q.; Cheong, W. C.; Wang, Y.; Zheng, L.; Xiao, H.; Chen, C.; Wang, D.; Peng, Q.; Gu, L.; Han, X.; Li, J.; Li, Y. Direct observation of noble metal nanoparticles transforming to thermally stable single atoms. *Nat. Nanotechnol.* **2018**, *13*, 856−861.

(27) Zhou, H.; Zhao, Y.; Xu, J.; Sun, H.; Li, Z.; Liu, W.; Yuan, T.; Liu, W.; Wang, X.; Cheong, W. C.; Wang, Z.; Wang, X.; Zhao, C.;

Yao, Y.; Wang, W.; Zhou, F.; Chen, M.; Jin, B.; Sun, R.; Liu, J.; Hong, X.; Yao, T.; Wei, S.; Luo, J.; Wu, Y. Recover the activity of sintered supported catalysts by nitrogen-doped carbon atomization. *Nat. Commun.* **2020**, *11*, 335.

(28) Lin, L.; Chen, Z.; Chen, W. Single atom catalysts by atomic diffusion strategy. *Nano Res.* **2021**, DOI: 10.1007/s12274-021-3412-9.

(29) Xiong, H.; Datye, A. K.; Wang, Y. Thermally stable single-atom heterogeneous catalysts. *Adv. Mater.* **2021**, 2004319.

(30) Liu, J.-C.; Tang, Y.; Wang, Y.-G.; Zhang, T.; Li, J. Theoretical understanding of the stability of single-atom catalysts. *Natl. Sci. Rev.* **2018**, *5*, 638−641.

(31) Yao, Y.; Huang, Z.; Xie, P.; Wu, L.; Ma, L.; Li, T.; Pang, Z.; Jiao, M.; Liang, Z.; Gao, J.; He, Y.; Kline, D. J.; Zachariah, M. R.; Wang, C.; Lu, J.; Wu, T.; Li, T.; Wang, C.; Shahbazian-Yassar, R.; Hu, L. High temperature shockwave stabilized single atoms. *Nat. Nanotechnol.* **2019**, *14*, 851−857.

(32) Zhang, E. H.; Wang, T.; Yu, K.; Liu, J.; Chen, W. X.; Li, A.; Rong, H. P.; Lin, R.; Ji, S. F.; Zhene, X. S.; Wang, Y.; Zheng, L. R.; Chen, C.; Wang, D. S.; Zhang, J. T.; Li, Y. D. Bismuth single atoms resulting from transformation of metal-organic frameworks and their use as electrocatalysts for CO_2 reduction. *J. Am. Chem. Soc.* **2019**, *141*, 16569−16573.

(33) Ma, Y.; Ren, Y.; Zhou, Y.; Liu, W.; Baaziz, W.; Ersen, O.; Pham-Huu, C.; Greiner, M.; Chu, W.; Wang, A.; Zhang, T.; Liu, Y. High-Density and thermally stable palladium single-atom catalysts for chemoselective hydrogenations. *Angew. Chem., Int. Ed.* **2020**, *59*, 21613−21619.

(34) Ji, S.; Jiang, B.; Hao, H.; Chen, Y.; Dong, J.; Mao, Y.; Zhang, Z.; Gao, R.; Chen, W.; Zhang, R.; Liang, Q.; Li, H.; Liu, S.; Wang, Y.; Zhang, Q.; Gu, L.; Duan, D.; Liang, M.; Wang, D.; Yan, X.; Li, Y. Matching the kinetics of natural enzymes with a single-atom iron nanozyme. *Nat. Catal.* **2021**, *4*, 407−417.

(35) Fan, Y.; Liu, S.; Yi, Y.; Rong, H.; Zhang, J. Catalytic nanomaterials toward atomic levels for biomedical applications: from metal clusters to single-atom catalysts. *ACS Nano* **2021**, *15*, 2005−2037.

(36) Banerjee, R.; Phan, A.; Wang, B.; Knobler, C.; Furukawa, H.; O'Keeffe, M.; Yaghi, O. M. High-throughput synthesis of zeolitic imidazolate frameworks and application to CO_2 capture. *Science* **2008**, *319*, 939−943.

(37) Phan, A.; Doonan, C. J.; Uribe-Romo, F. J.; Knobler, C. B.; O'Keeffe, M.; Yaghi, O. M. Synthesis, structure, and carbon dioxide capture properties of zeolitic imidazolate frameworks. *Acc. Chem. Res.* **2010**, *43*, 58−67.

(38) Ma, Z.; Wu, L.; Han, K.; Han, H. Pt nanozyme for O-2 self-sufficient, tumor-specific oxidative damage and drug resistance reversal. *Nanoscale Hori.* **2019**, *4*, 1124−1131.

(39) Choi, H.; Son, S. E.; Hur, W.; Tran, V. K.; Lee, H.; Park, Y.; Han, D. K.; Seong, G. H. Electrochemical immunoassay for determination of glycated albumin using nanozymes. *Sci. Rep.* **2020**, *10*, 12.

(40) Liu, L.; Du, B.; Shang, C.; Wang, J.; Wang, E. Construction of surface charge-controlled reduced graphene oxide-loaded Fe_3O_4 and Pt nanohybrid for peroxidase mimic with enhanced catalytic activity. *Anal. Chim. Acta* **2018**, *1014*, 77−84.

(41) Ge, C.; Wu, R.; Chong, Y.; Fang, G.; Jiang, X.; Pan, Y.; Chen, C.; Yin, J.-J. Synthesis of Pt hollow nanodendrites with enhanced peroxidase-like activity against bacterial infections: implication for wound healing. *Adv. Funct. Mater.* **2018**, *28*, 1801484.

(42) Jiang, B.; Duan, D.; Gao, L.; Zhou, M.; Fan, K.; Tang, Y.; Xi, J.; Bi, Y.; Tong, Z.; Gao, G. F.; Xie, N.; Tang, A.; Nie, G.; Liang, M.; Yan, X. Standardized assays for determining the catalytic activity and kinetics of peroxidase-like nanozymes. *Nat. Protoc.* **2018**, *13*, 1506−1520.

(43) Naha, P. C.; Liu, Y.; Hwang, G.; Huang, Y.; Gubara, S.; Jonnakuti, V.; Simon-Soro, A.; Kim, D.; Gao, L. Z.; Koo, H.; Cormode, D. P. Dextran-coated iron oxide nanoparticles as biomimetic catalysts for localized and ph-activated biofilm disruption. *ACS Nano* **2019**, *13*, 4960−4971.

(44) Sun, D.; Pang, X.; Cheng, Y.; Ming, J.; Xiang, S.; Zhang, C.; Lv, P.; Chu, C.; Chen, X.; Liu, G.; Zheng, N. Ultrasound-switchable nanozyme augments sonodynamic therapy against multidrug-resistant bacterial infection. *ACS Nano* **2020**, *14*, 2063−2076.

(45) Tao, Y.; Ju, E. G.; Ren, J. S.; Qu, X. G. Bifunctionalized mesoporous silica-supported gold nanoparticles: intrinsic oxidase and peroxidase catalytic activities for antibacterial applications. *Adv. Mater.* **2015**, *27*, 1097−1104.

(46) Wang, W. S.; Li, B. L.; Yang, H. L.; Lin, Z. F.; Chen, L. L.; Li, Z.; Ge, J. Y.; Zhang, T.; Xia, H.; Li, L. H.; Lu, Y. Efficient elimination of multidrug-resistant bacteria using copper sulfide nanozymes anchored to graphene oxide nanosheets. *Nano Res.* **2020**, *13*, 2156−2164.

(47) Vatansever, F.; de Melo, W.; Avci, P.; Vecchio, D.; Sadasivam, M.; Gupta, A.; Chandran, R.; Karimi, M.; Parizotto, N. A.; Yin, R.; Tegos, G. P.; Hamblin, M. R. Antimicrobial strategies centered around reactive oxygen species - bactericidal antibiotics, photodynamic therapy, and beyond. *Fems Microbiol. Rev.* **2013**, *37*, 955−989.

(48) Halliwell, B. Antioxidants in human health and disease. *Annu. Rev. Nutr.* **1996**, *16*, 33−50.

(49) Kalyanaraman, B. Teaching the basics of redox biology to medical and graduate students: Oxidants, antioxidants and disease mechanisms. *Redox Biol.* **2013**, *1*, 244−257.

(50) Djoric, D.; Kristich, C. J. Oxidative stress enhances cephalosporin resistance of enterococcus faecalis through activation of a two-component signaling system. *Antimicrob. Agents Chemother.* **2015**, *59*, 159−169.